Adaptive spatial filtering for off-axis digital holographic microscopy based on region-recognition approach with iterative thresholding

Xuefei He [a], Chuong Vinh Nguyen [a, b], Mrinalini Pratap [c], Yujie Zheng [a], Yi Wang [a], David R. Nisbet [a], Melanie Rug [d], Alexander G. Maier [c], Woei Ming Lee *[a]

[a]Research School of Engineering, College of Engineering and Computer Science, Australian National University, Canberra ACT 2601, Australia; [b]ARC Centre of Excellence for Robotics Vision, College of Engineering and Computer Science, Australian National University, Canberra ACT 2601, Australia; [c]Research School of Biology, College of Medicine, Biology and Environment, The Australian National University, Canberra ACT 2601, Australia; [d]Centre for Advanced Microscopy, ANU College of Physical & Mathematical Sciences, The Australian National University, Canberra, ACT 2601, Australia

*Corresponding:*steve.lee@anu.edu.au*

ABSTRACT

Here we propose a region-recognition approach with iterative thresholding, which is adaptively tailored to extract the appropriate region or shape of spatial frequency. In order to justify the method, we tested it with different samples and imaging conditions (different objectives). We demonstrate that our method provides a useful method for rapid imaging of cellular dynamics in microfluidic and cell cultures.

Keywords: adaptive imaging, spatial filtering, digital holographic microscopy, phase reconstruction

1. INTRODUCTION

Phase contrast microscopy [1] enables the transformation of phase changes into intensity changes that allows clear observation of cellular boundaries, but remains a qualitative imaging tool. The emergence of quantitative phase imaging aims to extract information of specific optical height of biological samples. Holography [2] operates by projecting two equal copies of light into two separate paths, one undisturbed and the other perturbed (phase delay) by the sample or object. The two paths combine to reveal the amount of phase delay that is recorded on a photosensitive film. Phase delay represents the optical path length difference between the two copies of the beams, which is then used to retrieve the optical height of the object. Combining holography with microscopy and digital imaging devices, Digital holographic microscope (DHM) [3] records interference pattern that emerges from superposition of a reference wave front with that emerging from the microscopic sample. Both optical height and refractive index fluctuations are then used to quantify differences between biological samples [4, 5]. DHM has been utilized in many biological applications such as determination of cellular motility [6], morphology [7] and biomechanics [8]. DHM heavily relies on numerical calculations to accurately reconstruct the phase of the biological sample. The numerical steps used in off-axis DHM technique include: discrete 2D Fourier transform, spatial frequency filtering [9], numerical propagation, phase unwrapping and aberration correction [10]. To achieve high throughput diseases diagnosis, these numerical calculations should be programmed to be automated and adaptive to different sample and imaging conditions. The complexity lies in the spatial frequency filtering process. Since the distribution of spatial frequencies of different samples varies significantly, the filter window needs to change correspondingly for the precise extraction of the desired frequency orders (first orders). One straightforward filtering method for precise extraction is manually selecting the first order in spatial frequency domain. Obviously, this approach requires manual input for each hologram, which is therefore not suitable for automation. While there are some histogram analysis techniques [11, 12] aiming to provide adaptive filtering that still requires manual intervention unfortunately. Here we propose an adaptive filtering process based on iterative thresholding and region-based selection. This combination gradually selects the optimal frequency component boundary for different holograms, avoiding fixing a single thresholding level and without any subjective input. The method is shown to be automated and suitable for all standard experimental conditions i.e. field of view, sample density, orientation and spacing of interference fringes. Region-recognition is also used to extract quantitative phase

SPIE BioPhotonics Australasia, edited by Mark R. Hutchinson, Ewa M. Goldys, Proc. of SPIE Vol. 10013, 1001329 · © 2016 SPIE · CCC code: 0277-786X/16/$18 · doi: 10.1117/12.2242876

measurements of biological red blood cells (RBCs) infected and uninfected with malaria parasite. All the processes are conducted in a single loop, which allows the continuous imaging and controlled use of the user interface. In the following sections, we explain the steps taken to implement the region recognition and iterative thresholding process as well as the sample classification of RBCs.

2. EXPERIMENT SETUP

Interference is the intensity pattern of two coherent waves' superposition. In DHM, the two waves are object wave $O(\bar{r},t)$ and reference wave $R(\bar{r},t)$ [Eq. (1) and (2)]. Hence the interference pattern is rewritten as Eq. (3).

$$O(\bar{r},t) = |O| exp\left[j\left(-\omega t + \left(\vec{k}_o \cdot \vec{r}\right) + \varphi\right)\right] \tag{1}$$

$$R(\bar{r},t) = |R_0| exp\left[j\left(-\omega t + \left(\vec{k}_r \cdot \vec{r}\right)\right)\right] \tag{2}$$

$$I = O_0^2 + R_0^2 + |OR| exp\left(j(\varphi + (\vec{k}_o - \vec{k}_r)\cdot\vec{r})\right) + |RO| exp\left(-j(\varphi + (\vec{k}_r - \vec{k}_o)\cdot\vec{r})\right) \tag{3}$$

where ω indicates the angular frequency of both waves and $\vec{k}\cdot\vec{r}$ indicates the dot product of wave vector $\vec{k}$ (two waves interfere with each other with same incident angle) and optical length $\vec{r}$. Most importantly, the phase delay φ derived from the sample (*O*) that is recorded as a shift in the intensity pattern, which descripts the optical height of the sample. In off-axis system, the sample and reference beams interfere at a slightly different angle θ creating two separate wave vectors $\vec{k}_r$ and $\vec{k}_o$. The phase shifts are spatially separated in the frequency domain that makes it possible for single shot phase recovery and high speed imaging [13, 14].

Figure 1(a) shows an off-axis DHM setup built on an inverted microscope system (OLYMPUS IX70) using a continuous wave visible laser (λ = 632.8nm, Spectra Physics Model 127-3502 Stabilite Polarized Helium-Neon Laser). The output beam is first coupled into a single-mode optical fiber using a microscopy objective (MO1, numerical aperture (N.A. = 0.25), then divided into two separate beams through an optical fiber splitter (F-S, 1 x 4 single mode fiber optic couplers P/N: FCQ632-APC). The outputs of the fibre are collimated using fibre collimators (CO). The beam travelling through the sample [object beam $O(\bar{r},t)$, Eq. (1)] is focused by L3 (f = 200mm) onto the back focal plane of a second microscope objective (MO2, N.A. = 0.1) and collected by an imaging objective lens (MO3). There are two imaging objective lenses (MO3) used in our setup with N.A. = 1.25 and low N.A. = 0.25. The reference beam [sample beam $R(\bar{r},t)$ in Eq. (2)] is collimated and then expanded by lenses L1 (f = 30mm) and L2 (f = 100mm) and finally recombined with the sample beam by a non-polarizing beam splitter (BS, THORLABS CM-BS013) onto a charge coupled device (CCD) camera (Retiga-2000R Fast 1394 Color Cooled) by tube lens L8 built in microscope frame. Figure 1(b) shows experimental setup where the sample is placed in an inverted microscope system. The incident directions of reference and sample beams at the CCD plane are indicated by in Fig. 1(a) beside the CCD.

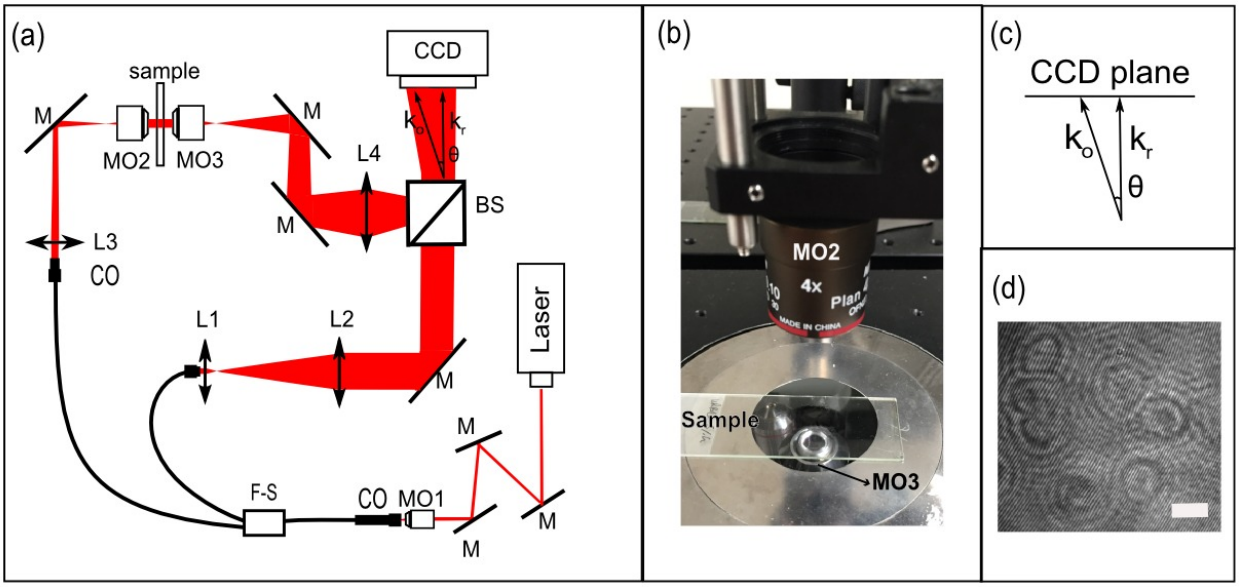

FIG. 1. DHM Imaging setup. (a) L1 and L2 expand the reference beam. L3 focuses object beam onto the back focal plane of a second microscope objective MO3. L4 is a tube lens. M are sliver-coated reflective mirrors to fold the beam along the imaging system. FS is fiber splitter and BS is the beam splitter for splitting and recombining the sample and reference beam. MO1 is the fiber coupling objective, MO2 is the illuminating objective and MO3 is the imaging objective. (b) Image showing the sample placed between the two objective lenses in the setup. (c) wave vectors of object wave and reference wave. (d) An example of a recorded hologram (scale bar = 5 μm).

3. REGION-RECOGNITION OF SPATIAL FREQUENCY

The spatial filtering process happens after fast Fourier transform (FFT) of the recorded hologram [Fig. 2(a)]. The phase shift is recorded in the spatial frequency on two symmetrical areas (+1 and -1 terms) in the frequency domain (FFT hologram) [Fig. 2(b)]. The shapes and sizes of these two symmetrical areas can vary according to different imaging conditions. First two columns in figure 4 give some examples that different samples and imaging conditions bring different symmetrical frequency components outlines. This implies that the frequency component needs to be carefully selected for accurate reconstruction. Here we propose an adaptive filtering process that is robust to all standard experimental conditions. The method is built upon an iterative thresholding and region-based selection. The procedures are broken down into 3 steps:

(1) Apply global threshold level (GTL) [15]to the intensity of FFT hologram to get the binary image[Fig. 2(c)] and then implement the region recognition process of it (*regionprops* MATLAB is used to provide three properties i.e. size of objects, centroid of objects in binary image and the box boundaries; *graythresh* MATLAB is used to get the GTL).

(2) Increase the threshold level by one percent of GTL and repeat the first step until the number of regions reaches three [Fig. 2(e)] (one for background intensity, one for the desired frequency component and one for the mirrored frequency component).

(3) Use box boundary data from *regionprops* function and the binary image form first step to get the right frequency component boundary and use it as a filtering window (additional Gaussian function is applied to smooth the edge of final filtering window).

Figure 2 shows an example of the adaptive filtering process. Figure 2(a) shows the recorded hologram of RBCs and Fig. 2(b) is the spatial frequency after FFT. Figures 2(c), (d) and (e) show the iterative threshold process with incremental threshold level. The processing time of this method is shown in Fig. 2(i). Once the appropriate spatial frequency is selected and centered [Fig. 2(g)], an inverse FFT (iFFT) is performed to retrieve the complex amplitude of the sample, which can be seen from Fig. 2(h). Since the phase map acquired from the recorded hologram is limited from $-\pi$ to π, so called wrapped, the true continuous phase value corresponding to the optical height of cells needs to be unwrapped [16]. Then we apply Zernike polynomials to compensate the aberration [10] in the system.

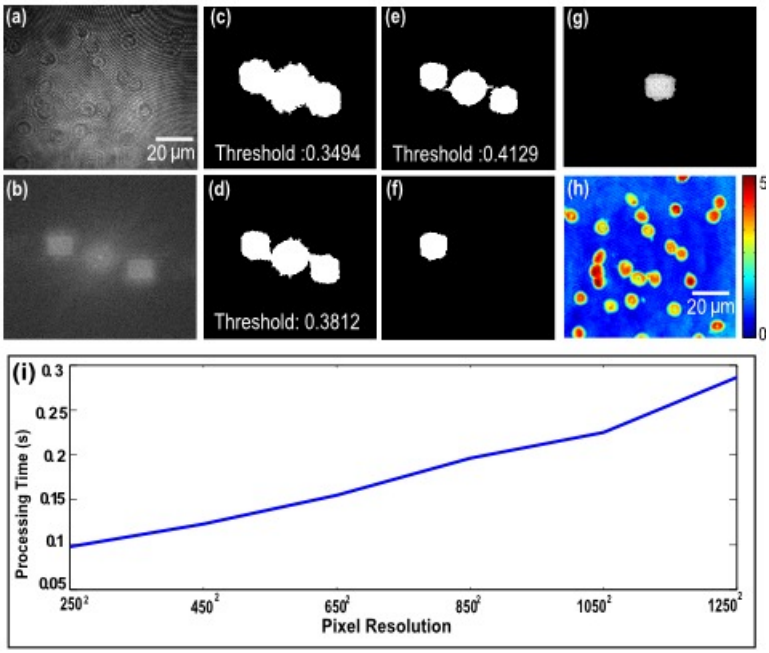

FIG. 2. The region-recognition method. (a) Recorded hologram of RBCs (b) Spatial frequency of the hologram after fast Fourier transform (FFT). (c), (d) and (e), shows intermediate iterative thresholding process with incremental threshold level. (f) Optimised spatial filter window (g) Final filtered and centred spatial frequency area. (h) Reconstructed phase image. The color bar gives the phase values by unit of radian. (i) Calculated time with different pixel size by this region-recognition method.

The only preset parameter in this process is the iterative threshold increment. To determine the proper iterative threshold increment, a highly scattering medium is prepared to test the filtering process. The sample [Fig. 3] is prepared with 50 μm polymer microspheres (Duke Scientific) deposited onto a thin film of opaque peptide hydrogel (Fmoc-FRGDF). The peptide hydrogel has been widely used in thick cell growth culture for neuronal growth. The scattering sample generates additional spatial frequency content that "blurs" the boundaries and "extends" the dimensions of three spatial frequencies components [FIG. 3. b]. That adds complexity to precise selection of first order frequency content for phase retrieval process. Figure 3 shows the sample schematic and different results under different threshold increments. From the results, the optimal increment is 1% of GTL, which is chosen as the preset iterative threshold increment in proposed filtering method. Figure 4 demonstrates the phase reconstruction process of different holograms when applying proposed filtering method. The figures have justified that the proposed adaptive filtering method has the ability automatically filtering out the proper frequency content from various holograms.

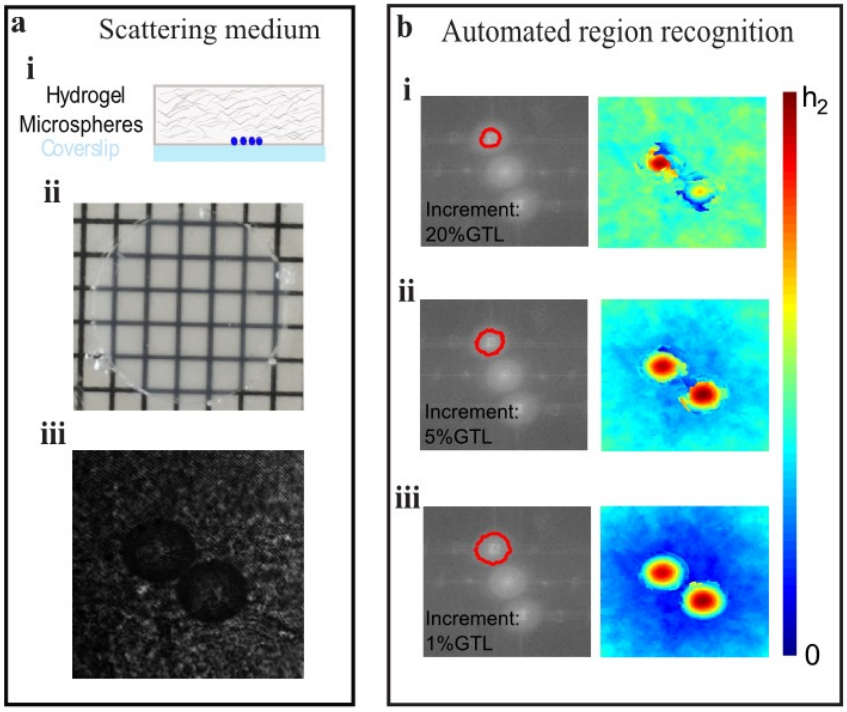

FIG. 3. Iterative threshold increment determination by scattering sample. a - i sample schematic, ii image of scattering medium taken from plan view with grid, iii acquired hologram. b - i, ii, iii show the different filter windows and the corresponding reconstructed phase of the microsphere. The threshold windows are created by setting different threshold increment in step (2), Fig.2 (j). Each threshold increment goes from 20%, 5% and 1% of GTL. The results show that 1% of GTL achieves an optimal filter window to retrieve an accurate reconstruction of the microsphere through a diffusive medium. Color bar h1 = h2 = 50 μm

From Fig 4, the proposed method has been tested using murine primary cortical neurons (cells that are adhesive, polymorphic, and relatively large), human RBCs (cells in suspension, biconcave and small) and microspheres (polystyrene, uniform structures of intermediate size). Figures 4(a), (b) and (c) show the hologram, FFT image and phase reconstruction of murine primary cortical neurons. The hologram was taken under 10X objective (N.A. 0.25) with fringes 45 degrees to the right in fine spacing (3 pixels per one fringe). Figures 4(d), (e) and (f) show the hologram, FFT image and phase reconstruction of a single RBC taken under high magnification (100 X, N.A 1.25 objective) with 15 pixels per one fringe. Figures 4(g), (h) and (i) show the hologram, FFT image and phase reconstruction of a single 6 □m polymer microsphere with fringes oriented inclined at 30 degrees with 8 pixels per one fringe. Figures 4 (j), (k) and (s) show the hologram, FFT image and phase reconstruction of a C17.2 cell line taken under 10X objective (N.A. 0.25) with fringes 30 degrees to the right in fine spacing with 4 pixels per one fringe. These results show that the iterative thresholding and region-recognition method can process a diverse range of shapes of spatial frequencies.

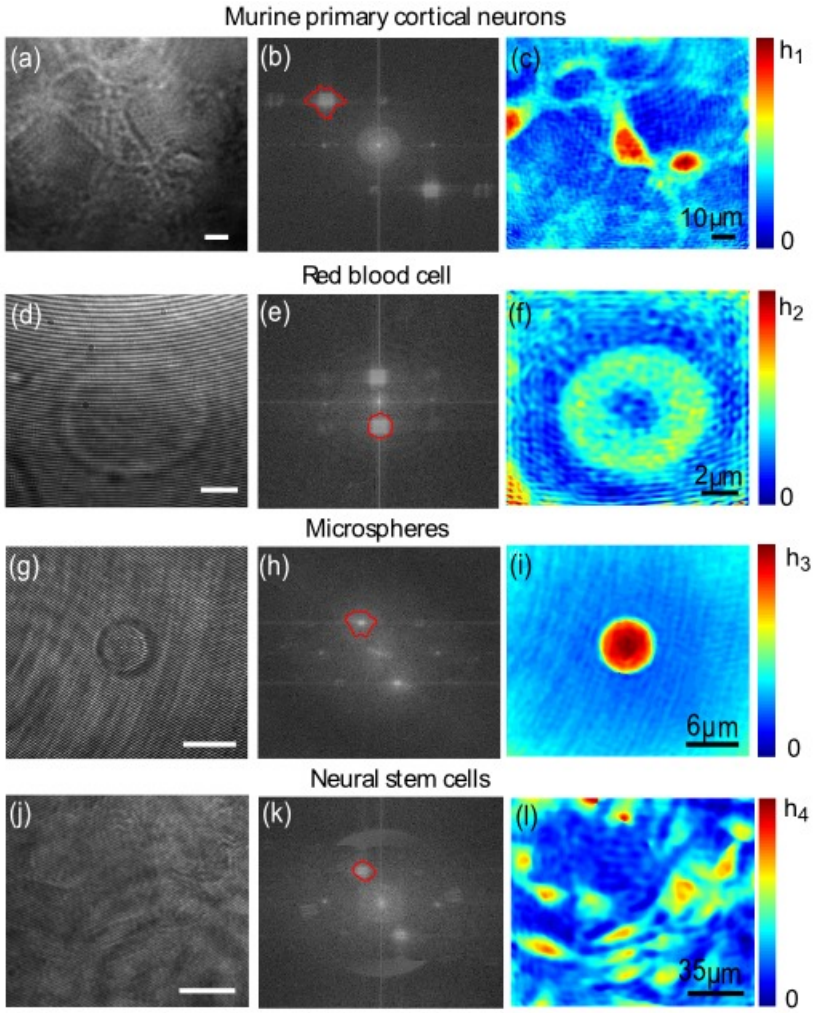

FIG. 4. Application of the region-recognition method under different experimental conditions. The first row depicts neuronal cortical cells (hologram (a), FFT image (b) and phase reconstruction (c)). The second row shows a single RBC as hologram (d), FFT image (e) and phase reconstruction (f). The third row presents 6µm microsphere on the microscopy slide (g), FFT image (h) and phase reconstruction (i). The last row presents C17.2 neural stem cell as hologram (j), FFT image (k) and phase reconstruction (l). The color bars in all phase reconstructions indicate h_1=10 µm, h_2= 2.9µm, h_3= 6.6µm, h_2 =13.3µm.

CONCLUSION

DHM relies heavily on accurate execution of numerical processes to reconstruct the phase of the biological sample. While off-axis DHM technique is perhaps the fastest holographic imaging technique, the accurate filtering of the spatial frequency can affect the final reconstructed image. We demonstrated that the combination of region-recognition and iterative thresholding conducted in a single loop can aid in selecting the optimal spatial frequency components with marginal delay (~0.1 to 0.3s). More importantly, as compared with past techniques, we showed that this technique can operate well in a turbid system, thus providing potential flexibility for imaging cellular processes in thick cell culture [17]. In the next step, we will aim to conduct live cell imaging in confluent cell cultures.

REFERENCES

[1] F. Zernike, "Phase contrast, a new method for the microscopic observation of transparent objects," Physica **9**, 686-698 (1942).
[2] D. Gabor, "A new microscopic principle," Nature **161**, 777-778 (1948).
[3] E. Cuche, Y. Emery, and F. Montfort, "Microscopy: One-shot analysis," Nat Photon **3**, 633-635 (2009).
[4] X. Yu, J. Hong, C. Liu, M. Cross, D. T. Haynie, and M. K. Kim, "Four-dimensional motility tracking of biological cells by digital holographic microscopy," Journal of biomedical optics **19**, 045001-045001 (2014).
[5] M. DaneshPanah, S. Zwick, F. Schaal, M. Warber, B. Javidi, and W. Osten, "3D holographic imaging and trapping for non-invasive cell identification and tracking," Display Technology, Journal of **6**, 490-499 (2010).
[6] P. Langehanenberg, L. Ivanova, I. Bernhardt, S. Ketelhut, A. Vollmer, D. Dirksen, G. Georgiev, G. von Bally, and B. Kemper, "Automated three-dimensional tracking of living cells by digital holographic microscopy," Journal of Biomedical Optics **14**, 014018-014018-014017 (2009).
[7] B. Rappaz, P. Marquet, E. Cuche, Y. Emery, C. Depeursinge, and P. Magistretti, "Measurement of the integral refractive index and dynamic cell morphometry of living cells with digital holographic microscopy," Opt. Express **13**, 9361-9373 (2005).
[8] Y. Park, M. Diez-Silva, G. Popescu, G. Lykotrafitis, W. Choi, M. S. Feld, and S. Suresh, "Refractive index maps and membrane dynamics of human red blood cells parasitized by Plasmodium falciparum," Proceedings of the National Academy of Sciences **105**, 13730-13735 (2008).
[9] E. Cuche, P. Marquet, and C. Depeursinge, "Spatial filtering for zero-order and twin-image elimination in digital off-axis holography," Applied Optics **39**, 4070-4075 (2000).
[10] T. Colomb, J. KŘhn, F. CharriŔre, C. Depeursinge, P. Marquet, and N. Aspert, "Total aberrations compensation in digital holographic microscopy with a reference conjugated hologram," Opt. Express **14**, 4300-4306 (2006).
[11] J. Li, Z. Wang, J. Gao, Y. Liu, and J. Huang, "Adaptive spatial filtering based on region growing for automatic analysis in digital holographic microscopy," Optical Engineering **54**, 031103-031103 (2015).
[12] J. Weng, H. Li, Z. Zhang, and J. Zhong, "Design of adaptive spatial filter at uniform standard for automatic analysis of digital holographic microscopy," Optik-International Journal for Light and Electron Optics **125**, 2633-2637 (2014).
[13] J. Hong, and M. K. Kim, "Single-shot self-interference incoherent digital holography using off-axis configuration," Optics letters **38**, 5196-5199 (2013).
[14] L. Xue, J. Lai, S. Wang, and Z. Li, "Single-shot slightly-off-axis interferometry based Hilbert phase microscopy of red blood cells," Biomed. Opt. Express **2**, 987-995 (2011).
[15] N. Otsu, "A threshold selection method from gray-level histograms," Automatica **11**, 23-27 (1975).
[16] M. A. Herráez, D. R. Burton, M. J. Lalor, and M. A. Gdeisat, "Fast two-dimensional phase-unwrapping algorithm based on sorting by reliability following a noncontinuous path," Applied Optics **41**, 7437-7444 (2002).
[17] N. Pavillon, J. Kühn, C. Moratal, P. Jourdain, C. Depeursinge, P. J. Magistretti, and P. Marquet, "Early cell death detection with digital holographic microscopy," PloS one **7**, e30912 (2012).